RECOMMENDATION ITU-R P.681-6*

Propagation data required for the design of Earth-space land mobile telecommunication systems

(Question ITU-R 207/3)

(1990-1994-1995-1997-1999-2001-2003)

The ITU Radiocommunication Assembly,

considering

a) that for the proper planning of Earth-space land mobile systems it is necessary to have appropriate propagation data and prediction methods;

b) that the methods of Recommendation ITU-R P.618 are recommended for the planning of Earth-space telecommunication systems;

c) that further development of prediction methods for specific application to land mobile-satellite systems is required to give adequate accuracy in all regions of the world and for all operational conditions;

d) that, however, methods are available which yield sufficient accuracy for many applications,

recommends

1 that the methods contained in Annex 1 be adopted for use in the planning of Earth-space land mobile telecommunication systems, in addition to the methods recommended in Recommendation ITU-R P.618.

Annex 1

1 Introduction

Propagation effects in the land mobile-satellite service (LMSS) differ from those of the fixed-satellite service (FSS) primarily because of the greater importance of terrain effects. In the FSS it is generally possible to discriminate against multipath, shadowing and blockage through the use of highly directive antennas placed at unobstructed sites. Therefore, in general, the LMSS offers smaller link availability percentages than the FSS. The prime availability range of interest to system designers is usually from 80% to 99%.

This Annex deals with data and models specifically needed for predicting propagation impairments in LMSS links, which include tropospheric effects, ionospheric effects, multipath, blockage and shadowing. It is based on measurements at 1.5 GHz (L-band) and 870 MHz in the UHF band.

* This Recommendation should be brought to the attention of Radiocommunication Study Group 8.

2 Tropospheric effects

2.1 Attenuation

Signal losses in the troposphere are caused by atmospheric gases, rain, fog and clouds. Except at low elevation angles, tropospheric attenuation is negligible at frequencies below about 1 GHz, and is generally small at frequencies up to about 10 GHz. Above 10 GHz, the attenuation can be large for significant percentages of the time on many paths. Prediction methods are available for estimating gaseous absorption (Recommendation ITU-R P.676) and rain attenuation (Recommendation ITU-R P.618). Fog and cloud attenuation is usually negligible for frequencies up to 10 GHz.

2.2 Scintillation

Irregular variations in received signal level and in angle of arrival are caused by both tropospheric turbulence and atmospheric multipath. The magnitudes of these effects increase with increasing frequency and decreasing path elevation angle, except that angle-of-arrival fluctuations caused by turbulence are independent of frequency. Antenna beamwidth also affects the magnitude of these scintillations. These effects are observed to be at a maximum in the summer season. A prediction method is given in Recommendation ITU-R P.618.

3 Ionospheric effects

Ionospheric effects on Earth-to-space paths are addressed in Recommendation ITU-R P.531. Values of ionospheric effects for frequencies in the range of 0.1 to 10 GHz are given in Tables 1 and 2 of Recommendation ITU-R P.680.

4 Shadowing

4.1 Roadside tree-shadowing model

Cumulative fade distribution measurements at 870 MHz, 1.6 GHz and 20 GHz have been used to develop the extended empirical roadside shadowing model. The extent of trees along the roadside is represented by the percentage of optical shadowing caused by roadside trees at a path elevation angle of 45° in the direction of the signal source. The model is valid when this percentage is in the range of 55% to 75%.

4.1.1 Calculation of fading due to shadowing by roadside trees

The following procedure provides estimates of roadside shadowing for frequencies between 800 MHz and 20 GHz, path elevation angles from 7° up to 60°, and percentages of distance travelled from 1% to 80%. The empirical model corresponds to an average propagation condition with the vehicle driving in lanes on both sides of the roadway (lanes close to and far from the roadside trees are included). The predicted fade distributions apply for highways and rural roads where the overall aspect of the propagation path is, for the most part, orthogonal to the lines of roadside trees and utility poles and it is assumed that the dominant cause of LMSS signal fading is tree canopy shadowing (see Recommendation ITU-R P.833).

Parameters required are the following:

f: frequency (GHz)

θ: path elevation angle to the satellite (degrees)

p: percentage of distance travelled over which fade is exceeded.

Step 1: Calculate the fade distribution at 1.5 GHz, valid for percentages of distance travelled of $20\% \geq p \geq 1\%$, at the desired path elevation angle, $60° \geq \theta \geq 20°$:

$$A_L(p,\theta) = -M(\theta) \ln (p) + N(\theta) \quad (1)$$

where:

$$M(\theta) = 3.44 + 0.0975\ \theta - 0.002\ \theta^2 \quad (2)$$

$$N(\theta) = -0.443\ \theta + 34.76 \quad (3)$$

Step 2: Convert the fade distribution at 1.5 GHz, valid for $20\% \geq p \geq 1\%$, to the desired frequency, f (GHz), where 0.8 GHz $\leq f \leq$ 20 GHz:

$$A_{20}(p, \theta, f) = A_L(p, \theta) \exp\left\{1.5\left[\frac{1}{\sqrt{f_{1.5}}} - \frac{1}{\sqrt{f}}\right]\right\} \quad (4)$$

Step 3: Calculate the fade distribution for percentages of distance travelled $80\% \geq p > 20\%$ for the frequency range 0.85 GHz $\leq f \leq$ 20 GHz as:

$$A(p, \theta, f) = A_{20}(20\%, \theta, f)\frac{1}{\ln 4}\ln\left(\frac{80}{p}\right) \quad \text{for} \quad 80\% \geq p > 20\% \quad (5)$$

$$= A_{20}(p, \theta, f) \quad \text{for} \quad 20\% \geq p > 1\%$$

Step 4: For path elevation angles in the range $20° > \theta \geq 7°$, the fade distribution is assumed to have the same value as at $\theta = 20°$.

Figure 1 shows fades exceeded at 1.5 GHz versus elevation angles between 10° and 60° for a family of equal percentages between 1% and 50%.

4.1.1.1 Extension to elevation angles > 60°

The roadside shadowing model at frequencies of 1.6 GHz and 2.6 GHz can be extended to elevation angles above 60° with the following procedure:

– apply equations (1) to (5) at an elevation angle of 60° at the above frequencies;

– linearly interpolate between the value calculated for an angle of 60° and the fade values for an elevation angle of 80° provided in Table 1;

– linearly interpolate between the values in Table 1 and a value of zero at 90°.

FIGURE 1

Fading at 1.5 GHz due to roadside shadowing versus path elevation angle

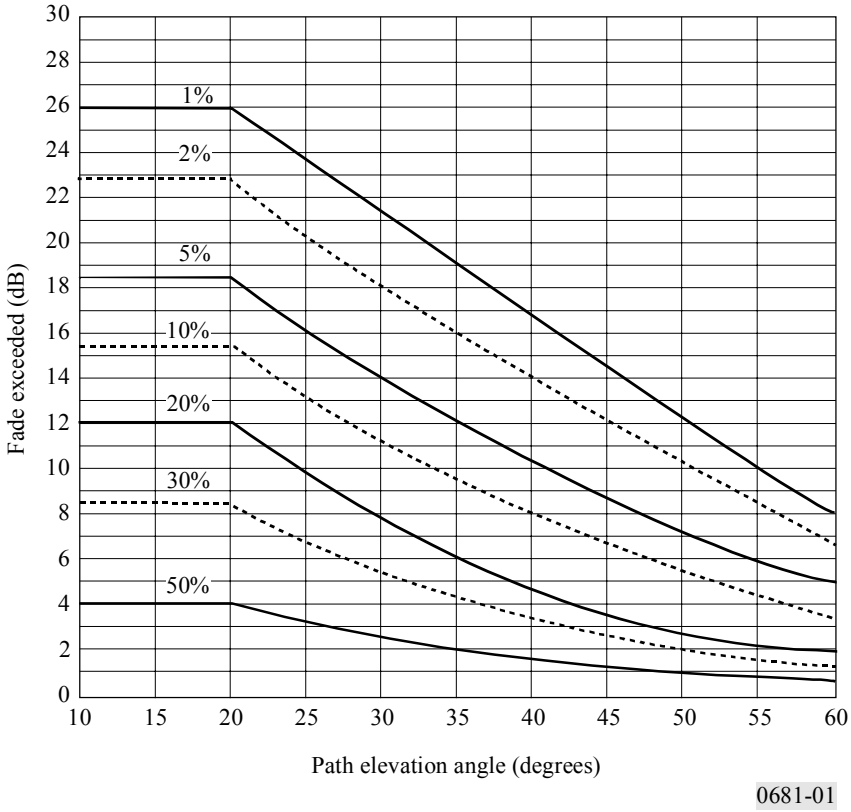

TABLE 1

Fades exceeded (dB) at 80° elevation

p (%)	Tree-shadowed	
	1.6 GHz	**2.6 GHz**
1	4.1	9.0
5	2.0	5.2
10	1.5	3.8
15	1.4	3.2
20	1.3	2.8
30	1.2	2.5

4.1.1.2 Application of roadside shadowing model to non-geostationary (non-GSO) and mobile-satellite systems

The prediction method above was derived for, and is applied to, LMSS geometries where the elevation angle remains constant. For non-GSO systems, where the elevation angle is varying, the link availability can be calculated in the following way:

a) calculate the percentage of time for each elevation angle (or elevation angle range) under which the terminal will see the spacecraft;

b) for a given propagation margin (ordinate of Fig. 1), find the percentage of unavailability for each elevation angle;

c) for each elevation angle, multiply the results of step a) and b) and divide by 100, giving the percentage of unavailability of the system at this elevation;

d) add up all unavailability values obtained in step c) to arrive at the total system unavailability.

If the antenna used at the mobile terminal does not have an isotropic pattern, the antenna gain at each elevation angle has to be subtracted from the fade margin in step b) above.

In the case of multi-visibility satellite constellations employing satellite path diversity (i.e. switching to the least impaired path), an approximate calculation can be made assuming that the spacecraft with the highest elevation angle is being used.

4.1.2 Fade duration distribution model

Optimal design of LMSS receivers depends on knowledge of the statistics associated with fade durations, which can be represented in units of travelled distance (m) or (s). Fade duration measurements have given rise to the following empirical model which is valid for distance fade duration $dd \geq 0.02$ m.

$$P(FD > dd \mid A > A_q) = \frac{1}{2}\left(1 - \text{erf}\left[\frac{\ln(dd) - \ln(\alpha)}{\sqrt{2}\,\sigma}\right]\right) \tag{6}$$

where $P(FD > dd \mid A > A_q)$ represents the probability that the distance fade duration, FD, exceeds the distance, dd (m), under the condition that the attenuation, A, exceeds A_q. The designation "erf" represents the error function, σ is the standard deviation of $\ln(dd)$, and $\ln(\alpha)$ is the mean value of $\ln(dd)$. The left-hand side of equation (6) was estimated by computing the percentage number of "duration events" that exceed dd relative to the total number of events for which $A > A_q$ in data obtained from measurements in the United States of America and Australia. The best fit regression values obtained from these measurements are $\alpha = 0.22$ and $\sigma = 1.215$.

Figure 2 contains a plot of P, expressed as a percentage, p, versus dd for a 5 dB threshold.

The model given by equation (6) is based on measurements at an elevation angle of 51° and is applicable for moderate to severe shadowing (percentage of optical shadowing between 55% and 90%). Tests at 30° and 60° have demonstrated a moderate dependence on elevation angle: the smaller the elevation angle, the larger is the fade duration for a fixed percentage. For example, the 30° fade duration showed approximately twice that for the 60° fade duration at the same percentage level.

4.1.3 Non-fade duration distribution model

A non-fade duration event of distance duration, dd, is defined as the distance over which the fade levels are smaller than a specified fade threshold. The non-fade duration model is given by:

$$p(NFD > dd \mid A < A_q) = \beta\,(dd)^{-\gamma} \tag{7}$$

where $p(NFD > dd \mid A < A_q)$ is the percentage probability that a continuous non-fade distance, NFD, exceeds the distance, dd, given that the fade is smaller than the threshold, A_q. Table 2 contains the values of β and γ for roads that exhibit moderate and extreme shadowing i.e. the percentage of optical shadowing of between 55% and 75% and between 75% and 90% respectively. A 5 dB fade threshold is used for A_q.

FIGURE 2

Best fit cumulative fade distribution for roadside tree shadowing with a 5 dB threshold

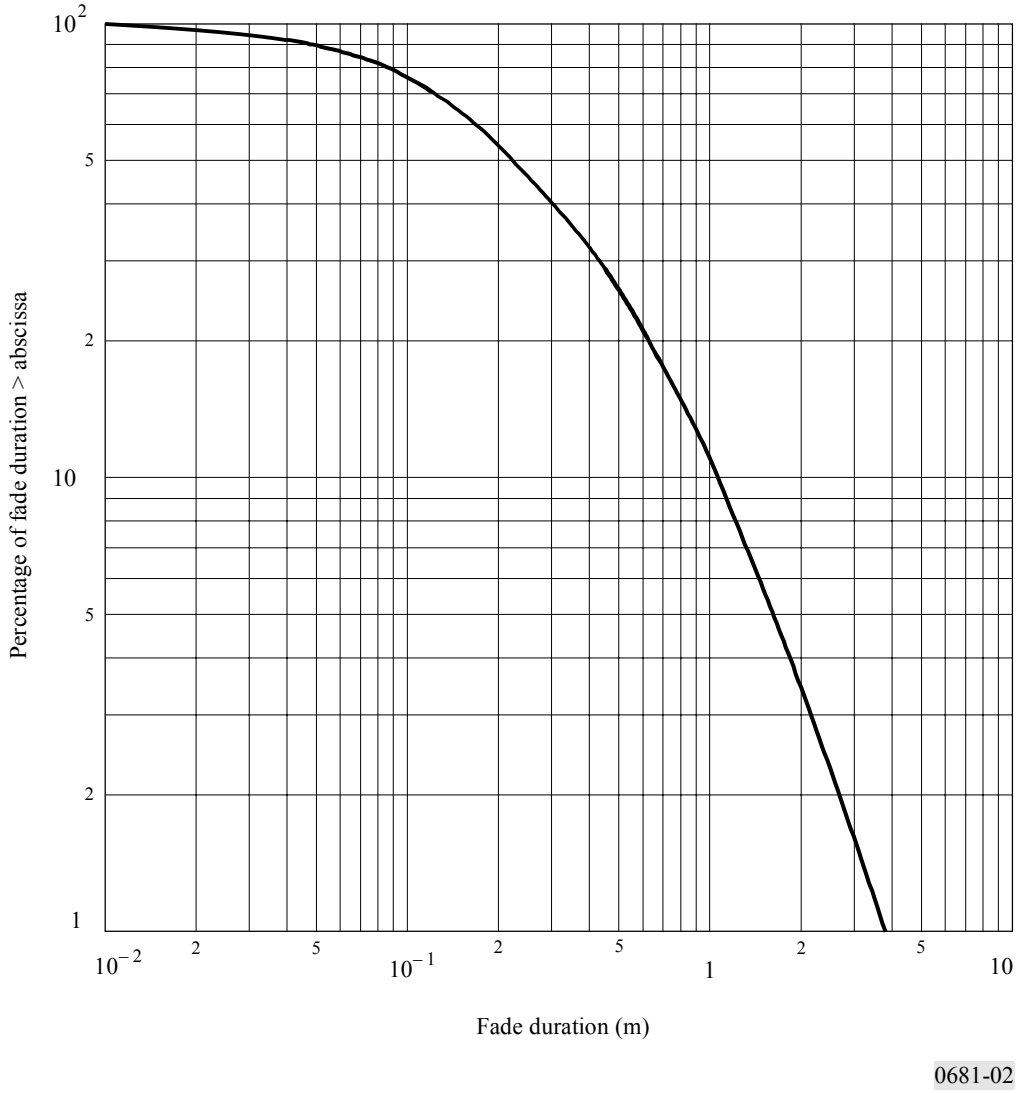

TABLE 2

Non-fade duration regression values for a 5 dB fade threshold at a path elevation angle of 51°

Shadowing level	β	γ
Moderate	20.54	0.58
Extreme	11.71	0.8371

4.2 Roadside building-shadowing model

Shadowing by roadside buildings in an urban area can be modelled by assuming a Rayleigh distribution of building heights. Figure 3 shows the geometry.

FIGURE 3

Geometry of roadside building shadowing model

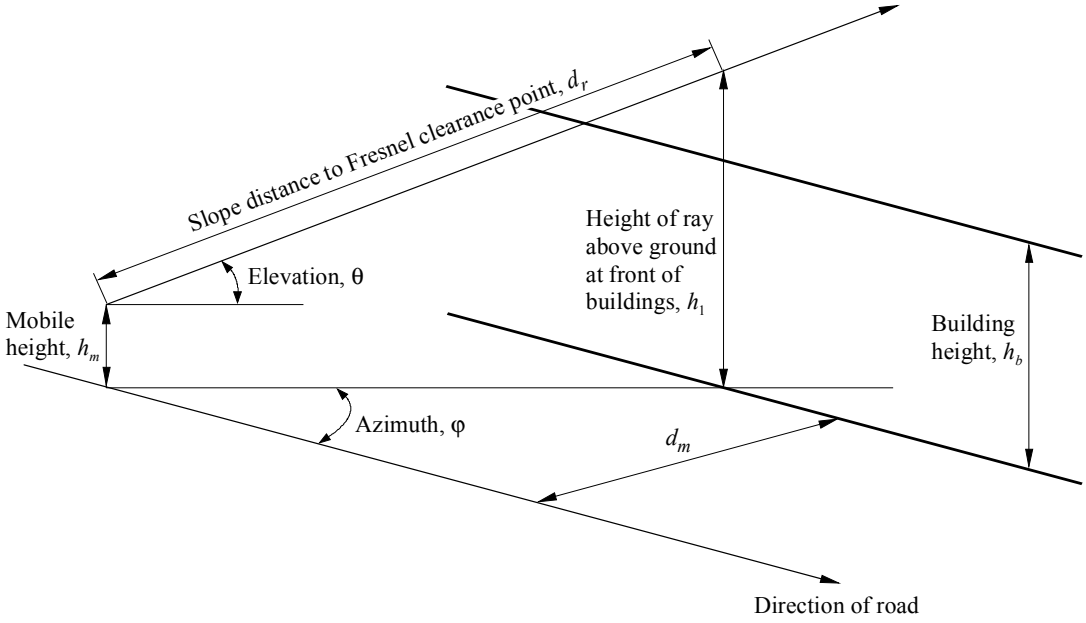

The percentage probability of blockage due to the buildings is given by:

$$p = 100 \exp\left[-(h_1 - h_2)^2 / 2h_b^2\right] \qquad \text{for} \quad h_1 > h_2 \tag{8}$$

where:

h_1: height of the ray above ground at the building frontage, given by:

$$h_1 = h_m + (d_m \tan\theta / \sin\varphi) \tag{8a}$$

h_2: Fresnel clearance distance required above buildings, given by:

$$h_2 = C_f \ (\lambda\, d_r)^{0.5} \tag{8b}$$

h_b: the most common (modal) building height

h_m: height of mobile above ground

θ: elevation angle of the ray to the satellite above horizontal

φ: azimuth angle of the ray relative to street direction

d_m: distance of the mobile from the front of the buildings

d_r: slope distance from the mobile to the position along the ray vertically above building front, given by:

$$d_r = d_m / (\sin\varphi \cdot \cos\theta) \tag{8c}$$

C_f: required clearance as a fraction of the first Fresnel zone

λ: wavelength

and where h_1, h_2, h_b, h_m, d_m, d_r and λ are in self-consistent units, and $h_1 > h_2$.

Note that equations (8a), (8b) and (8c) are valid for $0 < \theta < 90°$ and for $0 < \varphi < 180°$. The actual limiting values should not be used.

Figure 4 shows examples of roadside building shadowing computed using the above expressions for:

h_b = 15 m

h_m = 1.5 m

d_m = 17.5 m

Frequency = 1.6 GHz.

FIGURE 4

Examples of roadside building shadowing
(see text for parameter values)

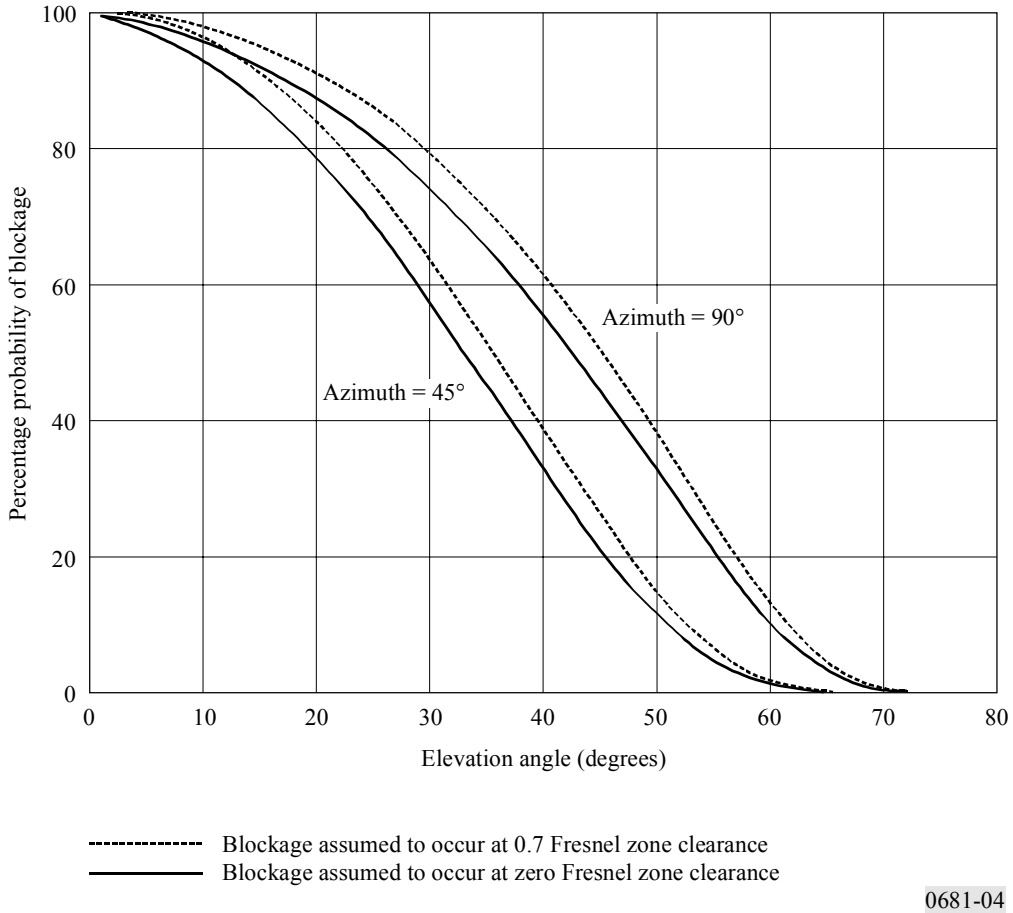

In Fig. 4 the dashed lines apply when blocking is considered to exist if the ray has a clearance less than 0.7 of the first Fresnel Zone vertically above the building front. The solid lines apply when blocking is considered to exist only when there is no line-of-sight.

Although the model indicates no blockage at the highest path elevation angles, users should be aware that occasional shadowing and blockage can occur from overpasses, overhanging standards, branches, etc.

4.3 Special consideration of hand-held terminals (user blockage)

When using hand-held communication terminals, the operator's head or body in the near-field of the antenna causes the antenna pattern to change. For the case of non-low Earth orbit (non-LEO) satellite systems (GSO, high Earth orbit (HEO), ICO), the user of the hand-held terminal is expected to be cooperative, i.e. to position himself in such a way as to avoid blockage from both the head (or body) and the environment. For LEO systems this assumption cannot be made. The influence of the head (or body) can be evaluated by including the modified antenna pattern (which has to be measured) in the link availability calculation as presented in § 4.1.1.2. Assuming that the azimuth angles under which the satellite is seen are evenly distributed, an azimuth-averaged elevation pattern can be applied. The small movements of the head or hand which lead to small variations in apparent elevation angle can also be averaged.

Relating to this effect, a field experiment was performed in Japan. Figure 5a shows the geometry of a human head and an antenna in the experiment. The satellite elevation angle is 32° and the satellite signal frequency is 1.5 GHz. The antenna gain is 1 dBi and the length is 10 cm. Figure 5b shows the variation of relative signal level versus azimuth angle φ in Fig. 5a. It can be seen from Fig. 5b that the maximum reduction in signal level due to user blockage is about 6 dB when the equipment is in the shadow region of the human head.

The results presented in Fig. 5b are intended to be illustrative only, since the data correspond to a single elevation angle and antenna pattern, and no account is taken of potential specular reflection effects, which may play a significant role in a hand-held environment where little directivity is provided.

Propagation data related to signal entry loss for reception within buildings and vehicles, of particular interest for hand-held terminals, may be found in Recommendation ITU-R P.679.

4.4 Modelling building blockage effects using street masking functions (MKF)

Building blockage effects can also be quantified using street MKFs indicating the azimuths and elevations for which a link can or cannot be completed. Functions of this type have often been obtained by means of photogrametric studies or ray-tracing. The MKF concept can be applied to simplified scenarios to produce a limited number of MKFs and hence, making it possible to produce fast, approximate assessments of the combined availability in different multi-satellite configurations.

A given urban area could be described, as a first approximation, by an average masking angle (MKA) (degrees).

The MKA is defined as the satellite elevation for grazing incidence with building tops when the link is perpendicular to the street or in mathematical terms:

$$MKA = \arctan\left(\frac{h}{w/2}\right) \quad \text{degrees} \tag{9}$$

where:

h: average building height

w: average street width.

Further, an urban scenario with a given MKA can be assumed to be made up of a combination of a small number of typical configurations (basic/constitutive scenarios), namely, street canyons (scy), street crossings (scr), T-junctions (T-j) and single walls (sw), each with a given occurrence probability (see Fig. 5). Similarly a path-mixture vector, $\vec{M}$, could be defined, stating, for a given built-up area, the probabilities of encountering each of the constitutive scenarios $\vec{M}$ (w_{scy}, w_{scr}, $w_{T\text{-}j}$, w_{sw}), with $\sum w_i = 1$. Input data to this model, i.e., MKA, can be obtained by observation of the environment or from city maps.

FIGURE 5

Basic/constitutive scenarios describing a given urban area

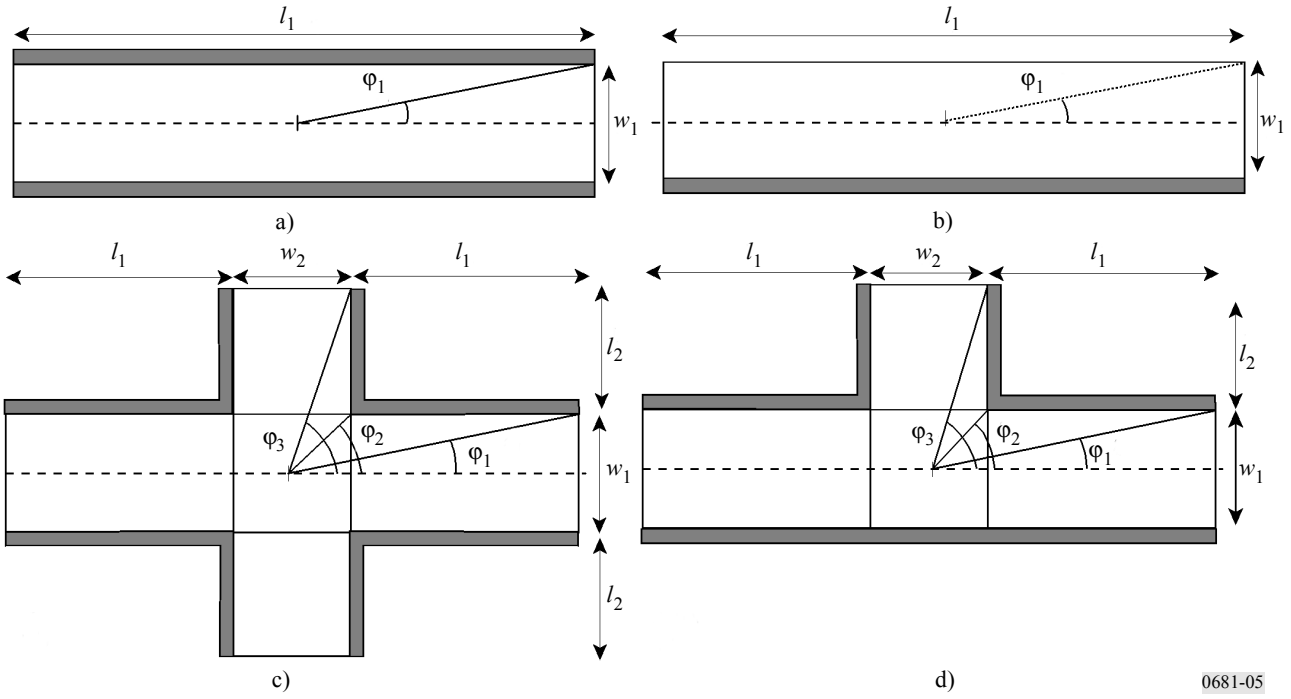

If availability probabilities are worked out for those four constitutive scenarios, the overall availability could be roughly estimated as the weighted sum of the availabilities in each scenario:

$$a_T = w_{scy}\, a_{scy} + w_{scr}\, a_{scr} + w_{T\text{-}j}\, a_{T\text{-}j} + w_{sw}\, a_{sw} \tag{10}$$

The MKFs for these four basic scenarios have been constructed by means of simple geometry assuming the user is in the middle of the scene (see Fig. 5). Considering a simple on-off, or line-of-sight – non-line-of-sight, propagation model (as in § 4.2 for the zero Fresnel zone clearance case), the MKFs of the four constitutive urban scenarios are presented in Fig. 6 where the ordinates indicate

elevation angles and the abscissas azimuths or, rather, street orientations, ξ, with respect to the link. The top half-plane indicates positive azimuths and the bottom half-plane corresponds to negative azimuths. A MKF indicates the regions in the celestial hemisphere where a link can be completed (non-shaded) or not (shaded areas). The contours delimiting the "forbidden" zones in the MKFs are defined by segments and points. The most relevant ones are illustrated in Fig. 6 and given by the following equations:

$$S_A: \quad \theta = \tan^{-1}\left(h \Big/ \sqrt{\left(\frac{w}{2}\right)^2 \left(\frac{1}{\tan^2 \varphi} + 1\right)} \right) \tag{11a}$$

$$P_A: \quad \left(\varphi_A = 90^\circ; \theta_A = \tan^{-1}\left(\frac{h}{w/2}\right) \right) \tag{11b}$$

$$S_{B_1}: \quad \theta = \tan^{-1}\left(h \Big/ \sqrt{\left(\frac{w_1}{2}\right)^2 \left(\frac{1}{\tan^2 \varphi} + 1\right)} \right) \tag{11c}$$

$$S_{B_2}: \quad \theta = \tan^{-1}\left(h \Big/ \sqrt{\left(\frac{w_1}{2}\right)^2 \left(\frac{1}{\tan^2 (90^\circ - \varphi)} + 1\right)} \right) \tag{11d}$$

$$P_B: \quad \left(\varphi_B = \tan^{-1}\left(\frac{w_1}{w_2}\right); \quad \theta_2 = \tan^{-1}\left(h \Big/ \sqrt{\left(\frac{w_1}{2}\right)^2 \left(\frac{1}{\tan^2 \varphi_B} + 1\right)} \right) \right) \tag{11e}$$

The availability for a particular basic scenario and a given geostationary (GSO) satellite can be computed by considering all possible street orientations, ξ, with respect to the user-satellite link. In Fig. 7 the position of a GSO satellite with respect to a T-junction is indicated. For the case illustrated in the Figure all possible orientations can be described by sweeping through all points in line A-B corresponding to a constant elevation angle and all possible street orientations. The availability is the fraction of the straight line A-B in the non-shaded part of the MKF. Similarly, a non-GSO orbit trajectory can be drawn on an MKF. The overall availability can be computed in this case by considering all possible street orientations with respect to all possible user-satellite link directions.

FIGURE 6

MKFs of a) a street canyon, b) a single wall, c) a street crossing and d) a T-junction

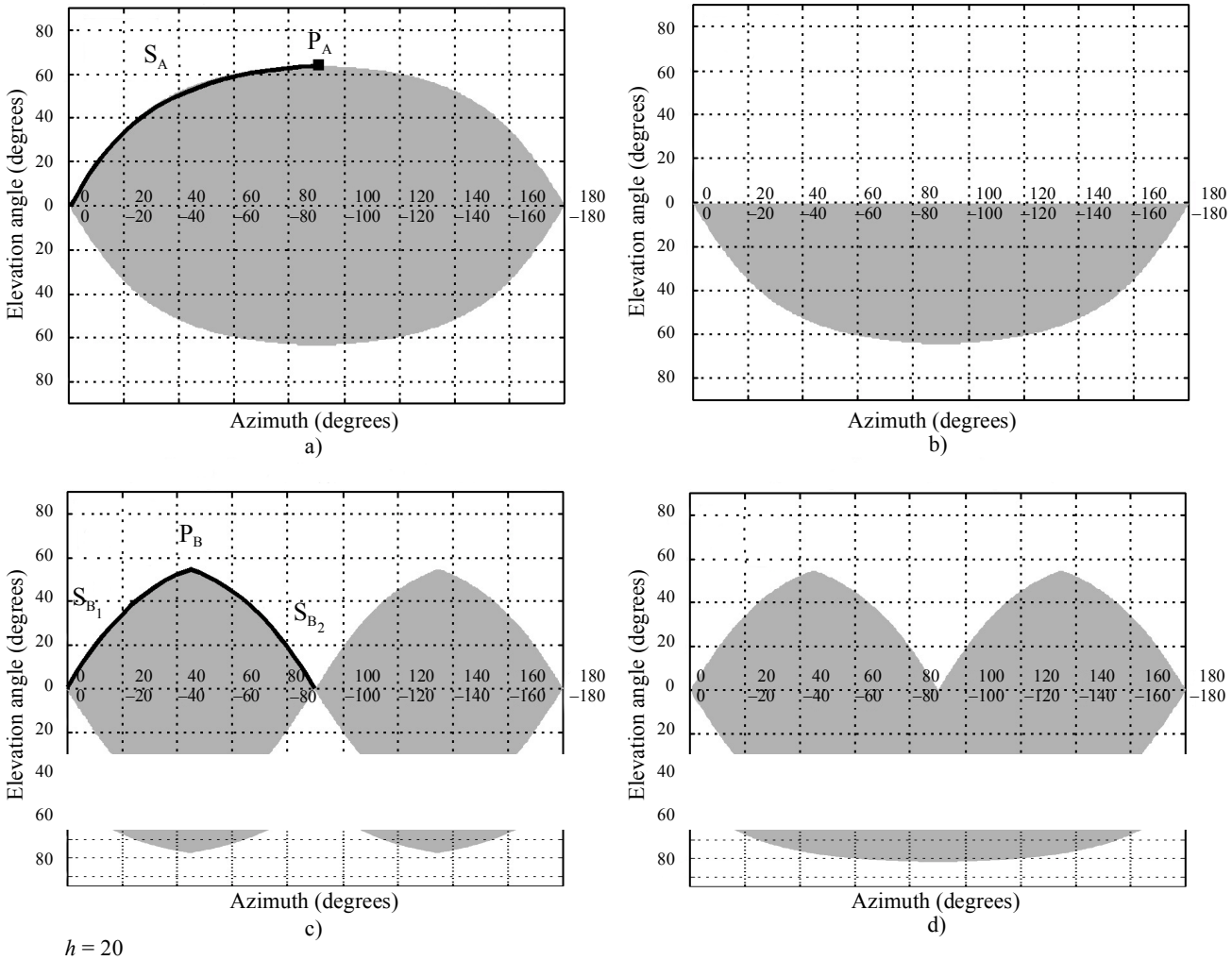

$h = 20$

$w_1 = 20$

$w_2 = 20$

MKA ≈ 63°

0681-06

FIGURE 7

Calculation of the availability for a T-junction and a GSO satellite

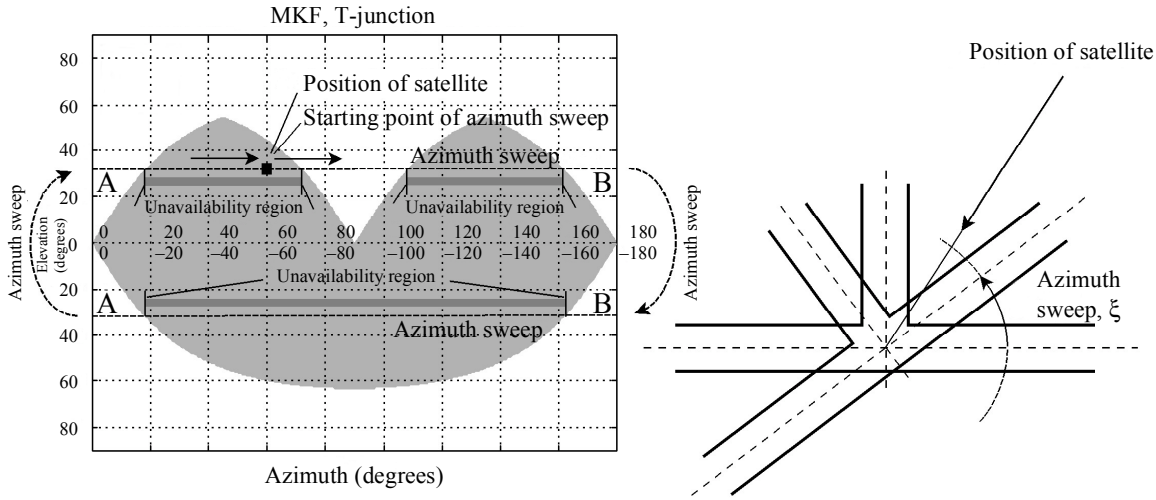

$h = 20$

$w_1 = 20$

$w_2 = 20$

MKA ≈ 63°

5 Multipath models for clear line-of-sight conditions

In many cases the mobile terminal has a clear line-of-sight (negligible shadowing) to the mobile satellite. Degradation to the signal can still occur under these circumstances, due to terrain-induced multipath. The mobile terminal receives a phasor summation of the direct line-of-sight signal and several multipath signals. These multipath signals may add constructively or destructively to result in signal enhancement or fade. The multipath signal characteristics depend on the scattering cross-sections of the multipath reflectors, their number, the distances to the receiving antenna, the field polarizations, and receiving antenna gain pattern.

The multipath degradation models introduced in the following sections are based on measurements made using an antenna with the following characteristics:

– omnidirectional in azimuth;

– gain variation between 15° and 75° elevation less than 3 dB;

– below the horizon (negative elevation angles) the antenna gain was reduced by at least 10 dB.

FIGURE 8a

Geometry of a human head and an antenna

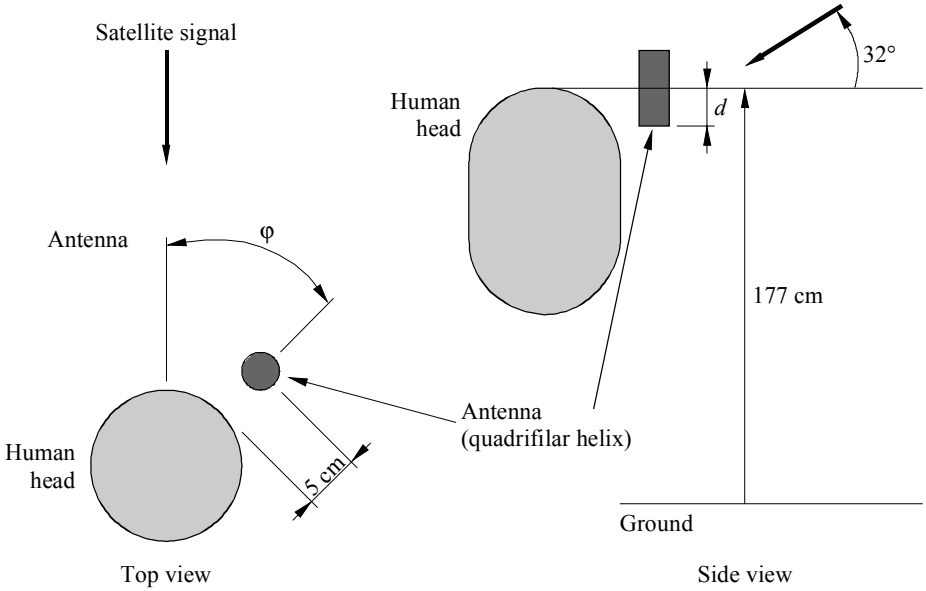

FIGURE 8b

Relative signal level corresponding to configuration of Fig. 8a

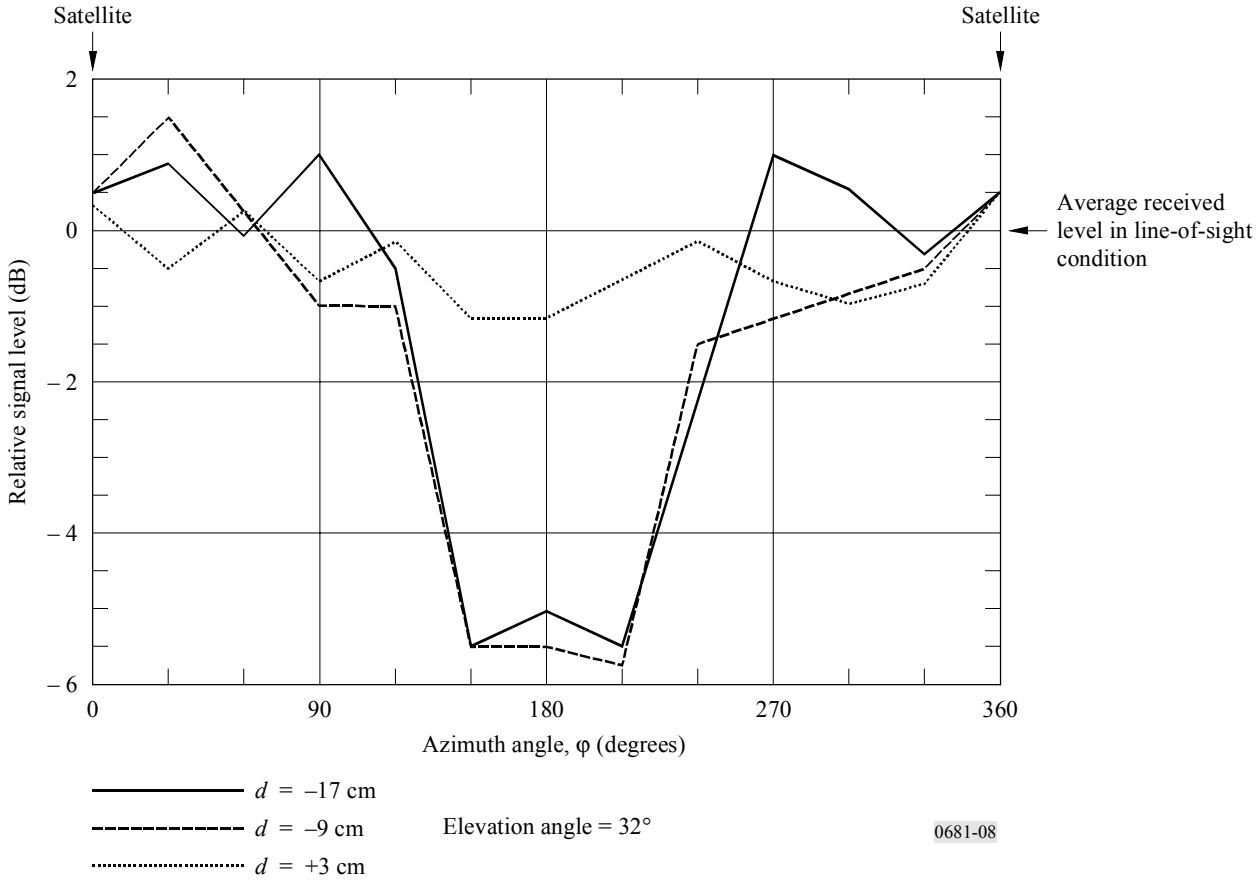

5.1 Multipath in a mountain environment

The distribution of fade depths due to multipath in mountainous terrain is modelled by:

$$p = a\, A^{-b} \tag{12}$$

for:

$$1\% < p < 10\%$$

where:

p: percentage of distance over which the fade is exceeded

A: fade exceeded (dB).

The curve fit parameters, a and b, are shown in Table 3 for 1.5 GHz and 870 MHz. Note that the above model is valid when the effect of shadowing is negligible.

TABLE 3

Parameters for best fit cumulative fade distribution for multipath in mountainous terrain

Frequency (GHz)	Elevation = 30°			Elevation = 45°		
	a	***b***	**Range (dB)**	***a***	***b***	**Range (dB)**
0.87	34.52	1.855	2-7	31.64	2.464	2-4
1.5	33.19	1.710	2-8	39.95	2.321	2-5

Figure 9 contains curves of the cumulative fade distributions for path elevation angles of 30° and 45° at 1.5 GHz and 870 MHz.

5.2 Multipath in a roadside tree environment

Experiments conducted along tree-lined roads in the United States of America have shown that multipath fading is relatively insensitive to path elevation over the range of 30° to 60°. The measured data have given rise to the following model:

$$p = u \exp(-vA) \tag{13}$$

for:

$$1\% < p < 50\%$$

where:

p: percentage of distance over which the fade is exceeded

A: fade exceeded (dB).

Note that the above model assumes negligible shadowing. The curve fit parameters, u and v, are shown in Table 4.

FIGURE 9

Best fit cumulative fade distributions for multipath fading in mountainous terrain

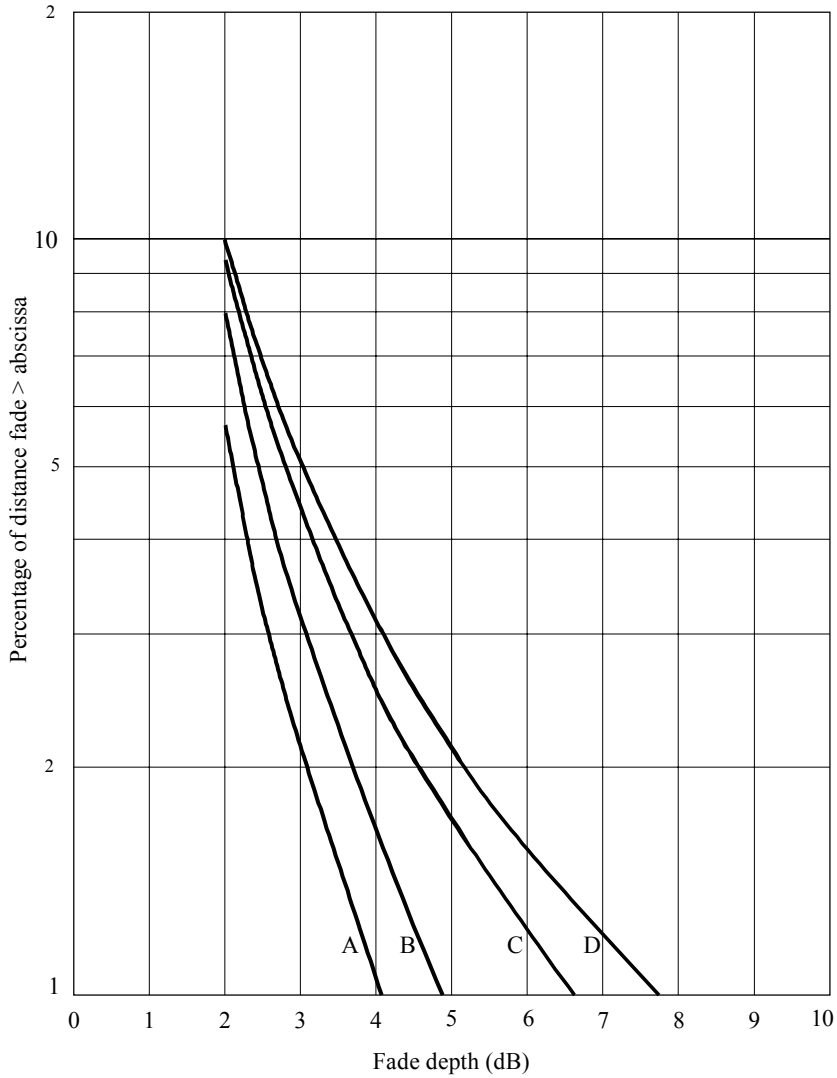

Curves A: 870 MHz, 45°
B: 1.5 GHz, 45°
C: 870 MHz, 30°
D: 1.5 GHz, 30°

0681-09

TABLE 4

Parameters for best exponential fit cumulative fade distributions for multipath for tree-lined roads

Frequency (GHz)	*u*	*v*	Fade range (dB)
0.870	125.6	1.116	1-4.5
1.5	127.7	0.8573	1-6

Figure 10 contains curves of the cumulative fade distributions for 1.5 GHz and 870 MHz. Enhanced fading due to multipath can occur at lower elevation angles (5° to 30°) where forward scattering from relatively smooth rolling terrain can be received from larger distances.

FIGURE 10

Best fit cumulative fade distributions for multipath fading on tree-lined roads

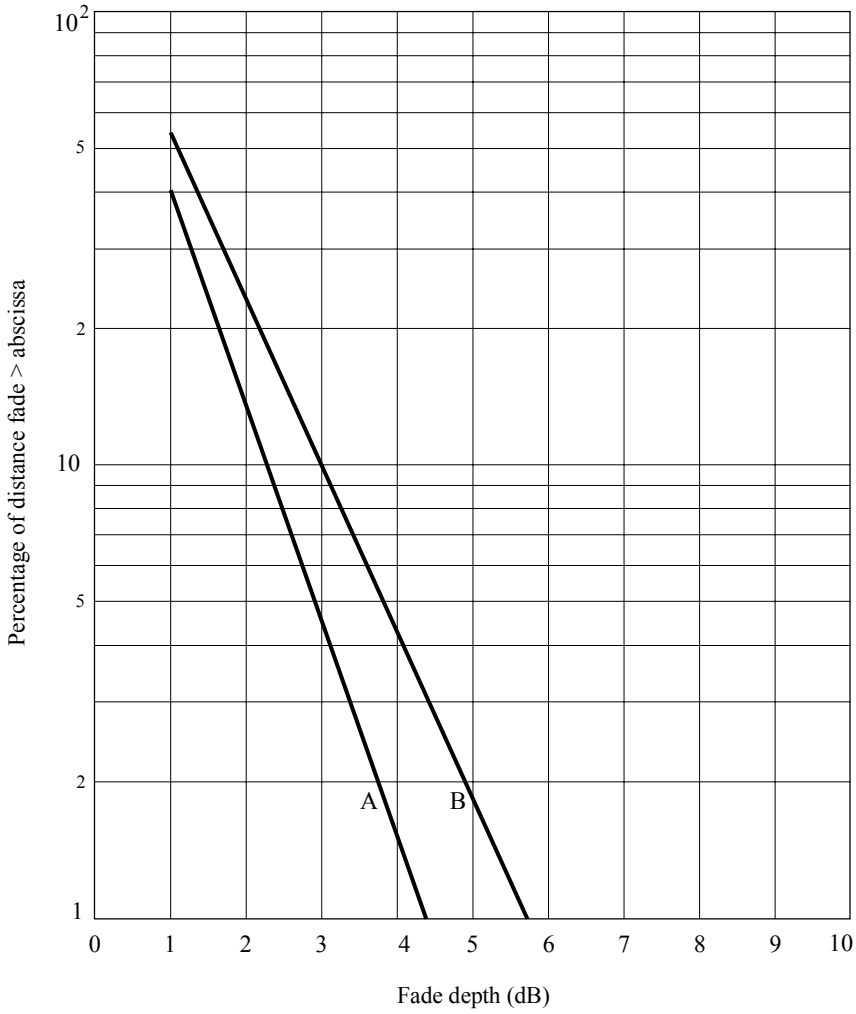

Curves A: 870 MHz
B: 1.5 GHz

0681-10

6 Statistical model for mixed propagation conditions

In § 4.1 and 5, models for specific conditions, that is, roadside shadowing conditions and clear line-of-sight conditions in a mountain environment and a roadside tree environment are given. In actual LMSS propagation environments such as urban and suburban areas, a mixture of different propagation conditions can occur. The cumulative distribution function (CDF) of signal levels in such mixed conditions can be calculated based on the following three-state model which is composed of a clear line-of-sight condition, a slightly shadowed condition and a fully blocked condition.

The long-term variations in the received signal may be described by a chain of distinct states. The basic idea of hidden chains is shown in Fig. 11a). The position of the switch determines which of the stochastic process $x_i[n]$ is observed at the output, where each process represents a specific propagation scenario. The shorter-term variations within each state may be modelled by analogue-valued channel models. Three states are utilized to represent line-of-sight, shadowing and blockage. The random process $s[n]$ represents the switch position, whose state is characterized by a semi-Markov chain with state transition diagram depicted in Fig. 11b).

FIGURE 11

Generation of the observed sequence a) and state transition diagram of a semi-Markov chain b)

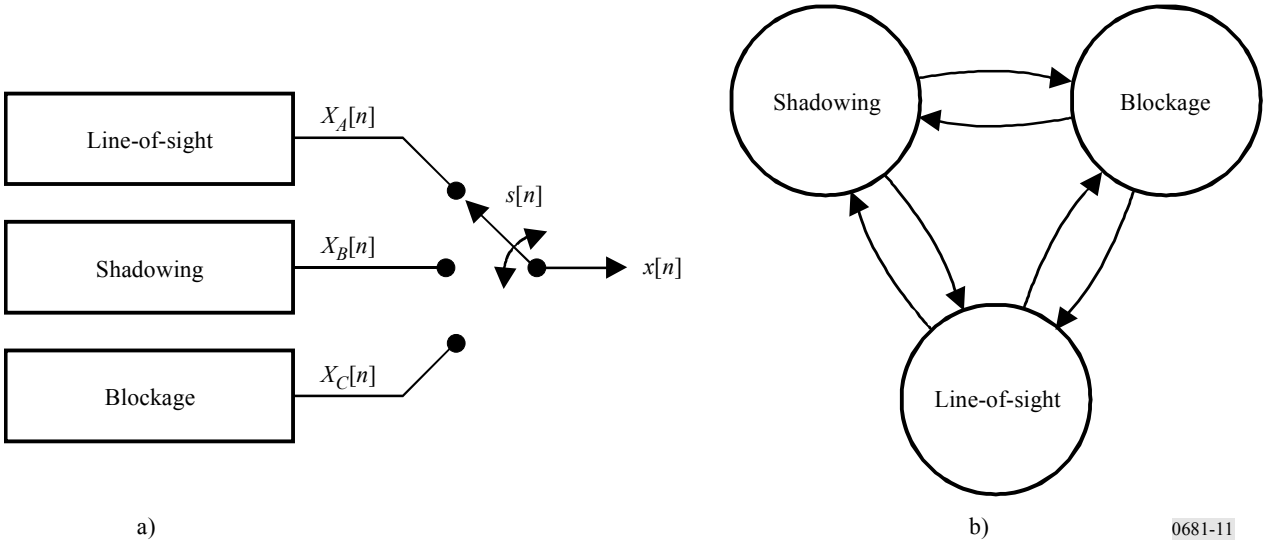

6.1 Prediction of fading statistics for a single satellite link

The following procedure provides estimates of overall fading statistics of the LMSS propagation link for frequencies up to 30 GHz with elevation angles from 10° to 90°. However, the suggested parameter values given here limit the applicable frequency range of 1.5 GHz to 2.5 GHz in urban and suburban areas. The receiving antenna gain assumed here is less than about 10 dBi.

Definition of the propagation states are as follows:

State A: clear line-of-sight condition

State B: slightly shadowed condition (by trees and/or small obstacles such as utility poles)

State C: fully blocked condition (by large obstacles such as mountains and buildings).

The following parameters are required:

P_A, P_B and P_C: occurrence probability of States A, B and C

$M_{r,A}$, $M_{r,B}$ and $M_{r,C}$: mean multipath power in States A, B and C

m and σ: mean and standard deviation of signal fading (dB) for the direct wave component in State B

θ: elevation angle (degrees).

Recommended values of the above parameters as a function of θ (degrees) are given as follows:

$$P_A = 1 - a\,(90 - \theta)^2 \qquad \text{for} \quad 10° \le \theta \le 90° \tag{14a}$$

where:

$$a = 1.43 \times 10^{-4} \quad \text{for urban area}$$
$$= 6.0 \times 10^{-5} \quad \text{for suburban area}$$

$$P_B = b\,P_C \tag{14b}$$

where:

$$b = 1/4 \quad \text{for urban area}$$
$$= 4 \quad \text{for suburban area}$$

and where:

$$P_C = (1 - P_A) / (1 + b) \tag{14c}$$

and

$$m = -10 \text{ dB} \qquad \sigma = 3 \text{ dB}$$

$$M_{r,B} = 0.03162\ (= -15 \text{ dB}) \qquad M_{r,C} = 0.01\ (= -20 \text{ dB})$$

The suggested value of $M_{r,A}$ depends on area types given below. For elevation angles between 10° and 45°, the value can be obtained with linear interpolation or extrapolation of the values in dB at θ = 30° and θ = 45°.

For an urban area:

$$M_{r,A} = 0.158\ (= -8 \text{ dB}) \qquad \text{for } \theta = 30°$$
$$= 0.100\ (= -10 \text{ dB}) \qquad \text{for } \theta \ge 45°$$

and for a suburban area:

$$M_{r,A} = 0.0631\ (= -12 \text{ dB}) \qquad \text{for } \theta = 30°$$
$$= 0.0398\ (= -14 \text{ dB}) \qquad \text{for } \theta \ge 45°$$

The step-by-step calculation procedure is as follows:

Step 1: Calculate the cumulative distribution of signal level x in State A ($x = 1$ for the direct wave component):

$$f_A(x \le x_0) = \int_0^{x_0} \frac{2x}{M_{r,A}} \exp\left(-\frac{1 + x^2}{M_{r,A}}\right) I_0\left(\frac{2x}{M_{r,A}}\right) \mathrm{d}x \tag{15}$$

where I_0 is a modified Bessel function of the first kind and of zero order.

NOTE 1 – This distribution is the Nakagami-Rice distribution with $a = 1$ and $2\sigma^2 = M_{r,A}$ described in Recommendation ITU-R P.1057.

Step 2: Calculate the cumulative distribution of signal level x in State B:

$$f_B(x \le x_0) \frac{6.930}{\sigma M_{r,B}} \int_0^{x_0} x \int_\varepsilon^\infty \frac{1}{z} \exp\left[-\frac{[20\log(z) - m]^2}{2\sigma^2} - \frac{x^2 + z^2}{M_{r,B}}\right] I_0\left(\frac{2xz}{M_{r,B}}\right) \mathrm{d}z\ \mathrm{d}x \tag{16}$$

where ε is a very small value but not zero (ε = 0.001 is suggested).

NOTE 1 – This distribution is known as the Loo distribution.

Step 3: Calculate the cumulative distribution of signal level x in State C:

$$f_C(x \le x_0) = 1 - \exp\left(-\frac{x_0^2}{M_{r,C}}\right) \tag{17}$$

NOTE 1 – This distribution is the Rayleigh distribution with $2q^2 = M_{r,C}$ described in Recommendation ITU-R P.1057.

Step 4: CDF, where the signal level x is less than a threshold level x_0 with a probability P in mixed propagation conditions, can be given by:

$$P(x \le x_0) = P_A\ f_A + P_B\ f_B + P_C\ f_C \tag{18}$$

Figure 12 shows calculated examples of CDFs, for the parameter values given above, with probabilities converted to time percentage.

FIGURE 12

Calculated examples of fading depth in urban and suburban areas at elevation angles of 30° and 45° (1.5-2.5 GHz; antenna gain ≤ 10 dBi)

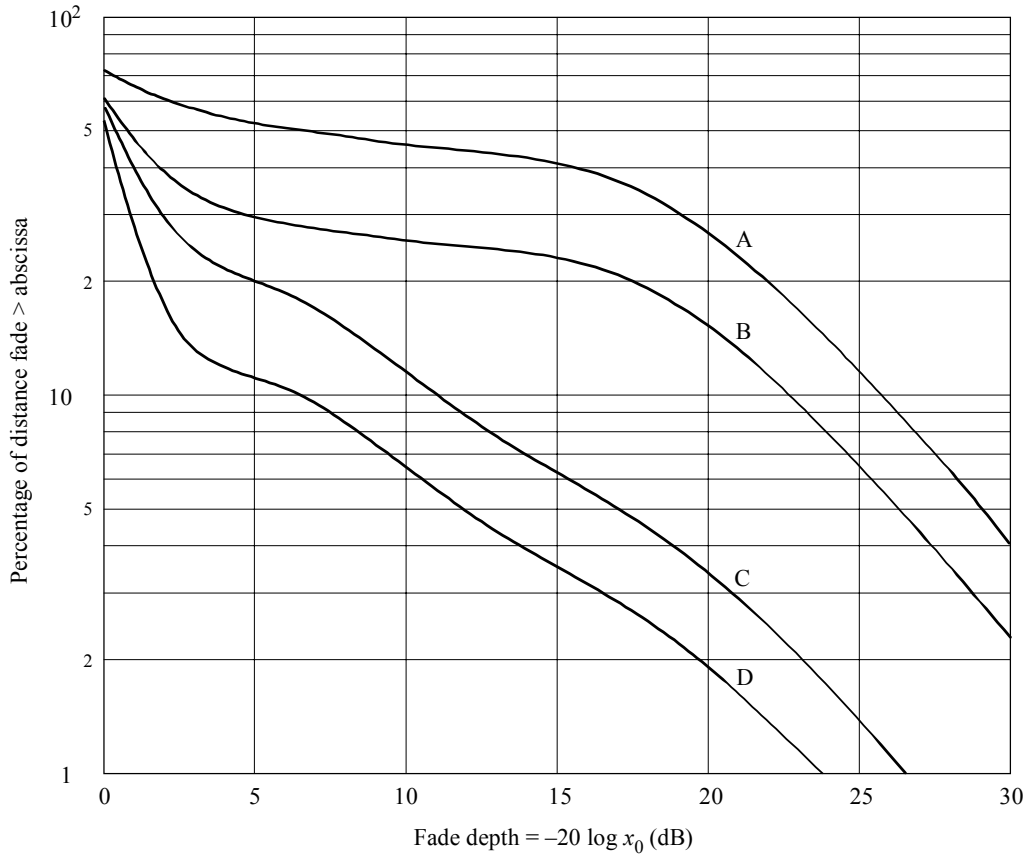

Curves A: urban, 30°
B: urban, 45°
C: suburban, 30°
D: suburban, 45°

0681-12

6.2 Prediction of state duration statistics for a single link

Simulation and performance estimation of LMSS receivers require knowledge of the time duration or equivalently the distance spent in each of three states classified as open, shadowed and blocked. Together with state transition probabilities, state duration distributions may be used in a semi-Markov state model to simulate the LMSS channel for a single GSO satellite.

The distribution of the state durations D (m) spent in each of the states A, B, and C, have been extracted from a set of roadside measurements at about 1.5 GHz with GSO satellites in the United Kingdom during the winter months. The measurements were taken in the suburbs of London in two different environments: a suburban environment with a mixture of open areas, lightly wooded roads and two-story houses; and a heavily wooded environment. The elevation angle towards the satellite was 29° for one set of suburban and wooded measurements (Suburban (I) and Wooded) and 13° for a second set of suburban measurements (Suburban (II)). The antenna was an omni-directional one mounted on a van. Threshold values of 5 and 10 dB were applied to the local average power level to sort the measurements into the three states (see Table 5).

Based on comparison with fade and non-fade durations given in § 4.1, the state duration distributions are as follows:

The power-law distribution for State A duration is:

$$P_A(D \le d) = 1 - \beta d^{-\gamma} \tag{19}$$

where the parameters β and γ depend on the degree of optical shadowing and $d > \beta^{1/\gamma}$.

The duration distribution for States B and C is a log-normal model valid for $d \ge 0.1$ m:

$$P_{B,C}(D \le d) = (1 + \text{erf}[(\ln(d) - \ln(\alpha)) / \sqrt{2\sigma}]) / 2 \tag{20}$$

where σ is the standard deviation of $\ln(d)$, $\ln(\alpha)$ is the mean value of $\ln(d)$ and the erf is as defined in Recommendation ITU-R P.1057.

The derived parameter values for the three-state duration distributions and the corresponding state transition probabilities are presented in Table 5.

TABLE 5

Parameters for state duration distributions and state transition probabilities

	State A		State B		State C		Transition probabilities					
Environment	β	γ	α	σ	α	σ	$P_{A\to B}$	$P_{A\to C}$	$P_{B\to A}$	$P_{B\to C}$	$P_{C\to A}$	$P_{C\to B}$
Suburban (I)	0.88	0.61	1.73	1.11	2.62	0.98	1	0	0.65	0.35	0	1
Suburban (II)	0.83	0.66	1.89	0.93	3.28	1.04	1	0	0.65	0.35	0	1
Wooded	0.60	0.84	2.05	1.05	1.55	1.02	1	0	0.42	0.58	0	1

7 Satellite diversity

In previous sections single satellite links have been considered. To improve availability, multiple satellite systems may use link diversity. The combination/switching of signals from various satellites is dealt with here. Two cases are considered, namely, the uncorrelated case where it is assumed that shadowing effects affecting received signals from visible satellites are uncorrelated, and the correlated case in which a given degree of correlation is present. In both situations multipath originated signal variations are assumed to be uncorrelated.

7.1 Uncorrelated case

The model in § 6 has a capability for assessing satellite diversity effects in the case of multivisibility satellite constellations (i.e. switching to the least impaired path). For GSO systems, the occurrence probabilities of each state for each satellite link, i.e. P_{An}, P_{Bn} and P_{Cn} (n = 1, 2, ..., N; N is number of visible satellites) depend on each satellite elevation θ_n State occurrence probabilities after the state-selection diversity, $P_{A:div}$, $P_{B:div}$ and $P_{C:div}$ are given by:

$$P_{A:div} = 1 - \prod_{n=1}^{N} [1 - P_{An}(\theta_n)] \tag{21a}$$

$$P_{B:div} = 1 - P_{A:div} - P_{C:div} \tag{21b}$$

$$P_{C:div} = \prod_{n=1}^{N} [P_{Cn}(\theta_n)] \tag{21c}$$

In the case of non-GSOs such as LEO and medium Earth orbit (MEO), the occurrence probabilities of the various states for each satellite link vary with time depending on the time-varying satellite elevation. The mean state occurrence probabilities, i.e. $\langle P_{A:div} \rangle$, $\langle P_{B:div} \rangle$ and $\langle P_{C:div} \rangle$, after operating satellite diversity from time t_1 to t_2 are as follows:

$$\langle P_{i:div} \rangle = \frac{1}{t_2 - t_1} \int_{t_1}^{t_2} P_{i:div}(t)\, \mathrm{d}t \qquad (i = A, B \text{ or } C) \tag{22}$$

By replacing P_A, P_B and P_C in equation (11) with $P_{A:div}$, $P_{B:div}$ and $P_{C:div}$ (in the case of GSO) or $\langle P_{A:div} \rangle$, $\langle P_{B:div} \rangle$ and $\langle P_{C:div} \rangle$, (in the case of non-GSO), the CDF after the state-selection satellite diversity can be calculated in a similar way. In this case, other parameter values should be kept constant at $\theta = 30°$ for provisional use.

7.2 Correlated case

In many instances, shadowing events affecting two links with a given angle spacing present some degree of correlation that needs to be quantified in order to produce more accurate estimations of the overall availability to be expected in a multiple satellite system. The shadowing cross-correlation coefficient is used for this purpose. This parameter may take up values in the range of ±1 going from positive, close to +1, for small angle spacing to even negative for larger spacing.

7.2.1 Quantification of the shadowing cross-correlation coefficient in urban areas

Here, a simple three-segment model to quantify the cross-correlation coefficient between shadowing events in urban areas is described. A canonical urban area geometry, the "street canyon" is used. The objective is the quantification of the cross-correlation coefficient $\rho(\gamma)$, with γ being the angle spacing between two separate satellite-to-mobile links in street canyons, which are described in terms of their MKA.

The geometry is indicated in Fig. 13 where:

θ_1, θ_2: satellite elevation angle

w: average street width

h: average building height

l: length of street under consideration.

FIGURE 13

Geometry of a street canyon

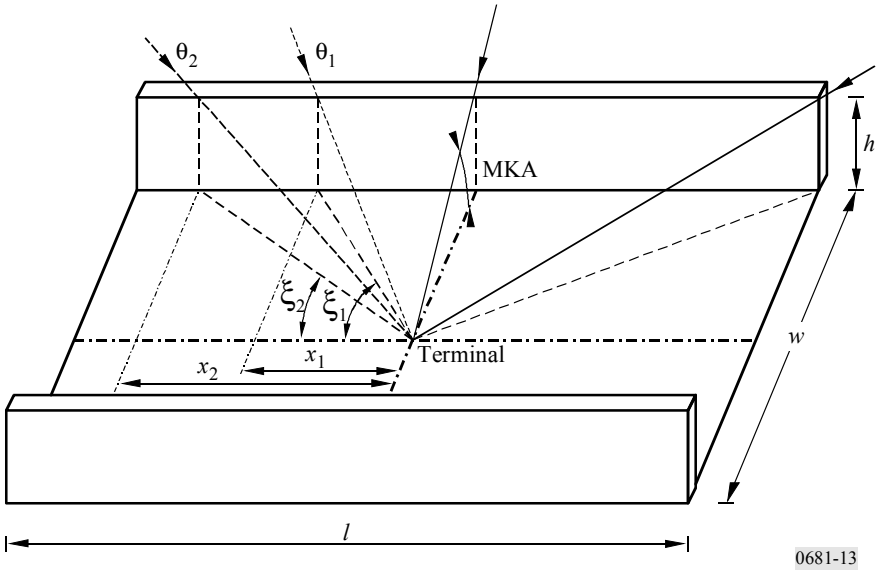

The angle spacing between two links, γ, can be put in terms of more convenient angles: the elevations of the two satellites, θ_i and θ_j, and their azimuth spacing, $\Delta\varphi$, i.e. the shadowing cross-correlation coefficient can be expressed as $\rho(\theta_i, \theta_j, \Delta\varphi)$.

Typical results obtained with this model are represented schematically in Fig. 14 which shows a general behaviour with a three-segment pattern defined by points A, B, C and D. In addition to this general pattern, there exist several special cases in which two or more of the four points merge.

Figure 14 shows that, in general, there usually exists a main lobe of positive, decreasing cross-correlation values for small azimuth spacing (typically $\Delta\varphi < 30^o$) while, for larger values of $\Delta\varphi$, the coefficient tends to settle at a constant negative value. The lobe will present higher maxima when the two satellites are at similar elevations. As the difference in elevations increases ($\theta_i >> \theta_j$), the lobe will show much lower maxima.

FIGURE 14

Three segment cross correlation coefficient model

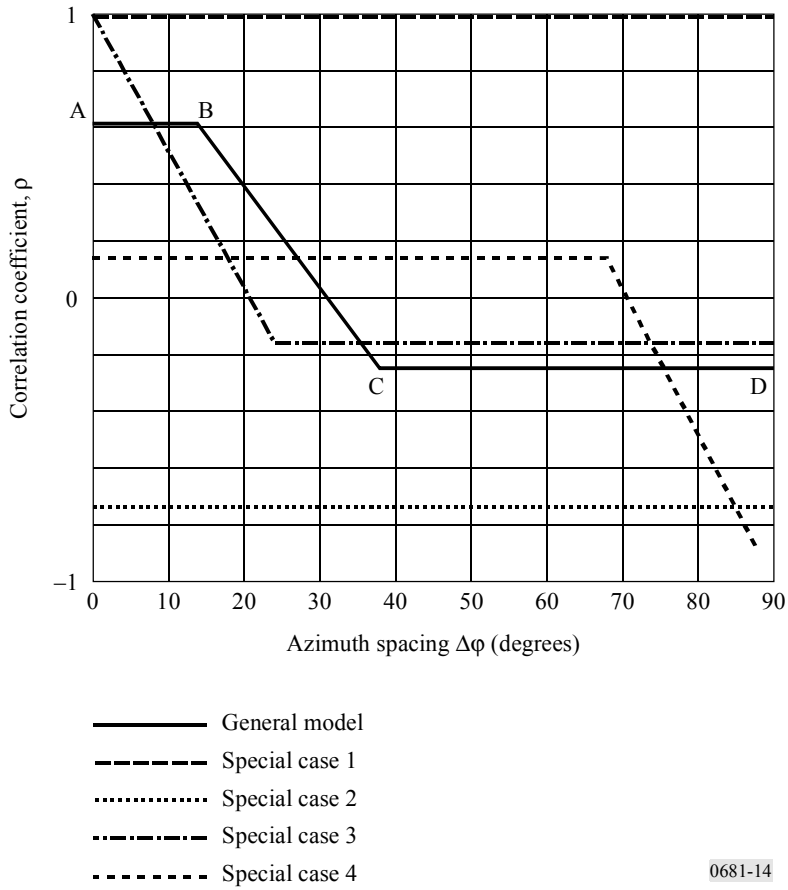

Special cases of this three-segment model have also been identified: special case 1 occurs when both satellites are above the MKA for any azimuth spacing. In this case, the correlation coefficient takes on a constant positive value of +1 for any $\Delta\varphi$. This is not a relevant case since, in this situation, satellite diversity is not required. Special case 2 occurs when one satellite is always above MKA and the other is always below (except at both ends of the canyon). In this case, the correlation coefficient takes on a constant negative value. Special case 3 occurs when the two satellites are at the same elevation. In this situation, the correlation lobe starts its decay from a maximum value of +1 (i.e. co-located satellites). This special case is applicable to those systems based on GSO satellites, widely spaced in azimuth, but with very similar elevations. Finally, special case 4 occurs for satellites with very different elevations ($\theta_i >> \theta_j$). Here, the correlation lobe extends across a much wider range of azimuth spacings but showing small positive correlation values.

It must be pointed out that, given the geometry of the scenario (street canyon) and that it is assumed that the user is in the middle of the street, correlation values are symmetric for all four $\Delta\varphi$ quadrants; this is the reason why only one quadrant is shown in Fig. 14.

With reference to Fig. 13, the following input data are used in the model: satellite elevations, θ_1 and θ_2 (degrees), average building height, h (m), average street width, w (m), and length of street under consideration, l (m). A large value is advised for this last parameter, i.e. $l \geq 200$ m. Further, it is assumed that $\theta_2 \geq \theta_1$. The model azimuth spacing, $\Delta\varphi$, resolution is 1° and is valid for all frequency bands although it becomes more accurate for bands above about 10 GHz.

The following steps shall be followed to calculate the cross-correlation coefficient values and azimuth spacings corresponding to model points A, B, C and D:

Step 1: Calculate auxiliary values x_1, x_2, M_1 and M_2 and angles ξ_1 and ξ_2 (see Fig. 13):

$$x_1 = \sqrt{\left(\frac{h}{\tan\theta_1}\right)^2 - \left(\frac{w}{2}\right)^2} \quad \text{and} \quad x_2 = \sqrt{\left(\frac{h}{\tan\theta_1}\right)^2 - \left(\frac{w}{2}\right)^2} \tag{23}$$

– If $(x_{1,2})^2 < 0$ go to Step 6. This situation occurs when satellite 1 and/or 2 are always in line-of-sight conditions for any azimuth spacing.

– If $x_{1,2} > l/2$, make $x_{1,2} = l/2$. This situation occurs when there is visibility for satellite 1 and/or 2 only at both ends of the street.

$$\xi_1 = \text{round}\left(\arctan\frac{w/2}{x_1}\right) \quad \text{and} \quad \xi_2 = \text{round}\left(\arctan\frac{w/2}{x_2}\right) \tag{24}$$

$$M_1 = \frac{\xi_1 + 0.5}{90} \quad \text{and} \quad M_2 = \frac{\xi_2 + 0.5}{90} \tag{25}$$

where "round" means rounded to the nearest integer value (degrees).

Step 2: Calculation of auxiliary information related to model points A and D.

For point A:

$$N_{11} = 4\xi_1 + 2 \quad N_{00} = 360 - 4\xi_2 - 2 \quad N_{01} = 4(\xi_2 - \xi_1) \quad N_{10} = 0 \tag{26}$$

For point D:

– If $\xi_1 + \xi_2 \leq 90$,

$$N_{11} = 0 \quad N_{00} = 360 - 4\xi_1 - 4\xi_2 - 4 \quad N_{01} = 4\xi_2 + 2 \quad N_{10} = 4\xi_1 + 2 \tag{27a}$$

– If $\xi_1 + \xi_2 > 90$,

$$N_{11} = 4\xi_1 + 4\xi_2 + 4 - 360 \quad N_{00} = 0 \quad N_{01} = 360 - 4\xi_1 - 2 \quad N_{10} = 360 - 4\xi_2 - 2 \tag{27b}$$

Step 3: Calculation of the cross-correlation coefficient at points A and D:

$$\rho_{A,D} = \frac{1}{359}\,\frac{N_{11}(1-M_1)(1-M_2) + N_{00}(0-M_1)(0-M_2) + N_{10}(1-M_1)(0-M_2) + N_{01}(0-M_1)(1-M_2)}{\sigma(\theta_1)\,\sigma(\theta_2)} \tag{28}$$

$$\sigma^2(\theta_1) = \frac{(4\xi_1 + 2)(1-M_1)^2 + (360 - 4\xi_1 - 2)(0-M_1)^2}{359} \tag{29a}$$

$$\sigma^2(\theta_2) = \frac{(4\xi_2 + 2)(1-M_2)^2 + (360 - 4\xi_2 - 2)(0-M_2)^2}{359} \tag{29b}$$

Step 4: At point B, the correlation coefficient is the same as at point A and its azimuth spacing, $\Delta\varphi$, is given by:

$$\text{Azimuth}_{\text{Point B}} = \xi_2 - \xi_1 \quad \text{degrees} \tag{30}$$

Step 5: At point C, the correlation coefficient is the same as at point D and its azimuth spacing, $\Delta\varphi$, is given by:

– If $\xi_1 + \xi_2 \leq 90$, $\text{Azimuth}_{\text{Point C}} = \xi_1 - \xi_2$ degrees (31a)

– If $\xi_1 + \xi_2 > 90$, $\text{Azimuth}_{\text{Point C}} = 180 - \xi_1 - \xi_2$ degrees (31b)

Step 6: This is the case in which, for one or both elevations, there are always line-of-sight conditions. Here, the correlation coefficient is calculated in a slightly different manner to that in Step 3:

– If both satellites are always visible, the cross-correlation coefficient is constant and equal to +1 for any $\Delta\varphi$.

– If one of the satellites is always visible, the cross-correlation coefficient is also constant and is given by:

$$\rho = \left(\frac{N_{11}}{180} - 1 \right) \tag{32}$$

where $N_{11} = 4\xi_1 + 2$, and ξ_1 is calculated as in Step 1.

7.2.2 Availability calculations

Once the cross-correlation coefficient is available, it is possible to compute the availability improvement introduced by the use of satellite diversity. Here, expressions to calculate the system availability for the two-satellite diversity case are provided. Given the usually small margins (or power control ranges) used in land mobile satellite systems, only shadowing effects need to be considered. This is a reasonable working hypothesis since availability events will correspond to links in line-of-sight conditions in which case multipath-originated variations are Ricean and thus, fairly small. In the case of shadowed conditions (heavy or light), the links will be in an outage state even if multipath gives rise to significant signal enhancements.

Given two angle spaced links with unavailability probabilities, p_1 and p_2, and a shadowing cross-correlation coefficient ρ, the overall availability improbability after satellite diversity is given by:

$$p_0 = \rho \sqrt{p_1(1 - p_1)} \sqrt{p_1(1 - p_2)} + p_1 p_2 \tag{33}$$

and the probability of availability will be $1 - p_0$. Valid values of ρ in equation (33) are limited to those rendering non-negative values for p_0. Probabilities p_1 and p_2, for urban areas can be computed by using the model given in § 4.2.

Overall calculations for a given time interval or for a complete constellation period require the computation of weighted averages over all positions (azimuths and elevations) of the two satellites with respect to the user terminal.

7.3 Modelling satellite diversity effects using MKFs

MKFs as defined in § 4.4 can be used in the calculation of multi-satellite availabilities. Possible partial correlation of blockage effects between the various links is already contained in the geometry of the masks themselves. In Fig. 15 the calculation of the availability of a system comprising two GSO satellites is illustrated. Lines A-B and C-D indicate the sweep paths to be followed for the calculation of the combined availability. Line A-B indicates the 360º azimuth sweep at elevation θ_1 corresponding to satellite-1 and line C-D indicates the 360º azimuth sweep at elevation θ_2 for satellite-2. To account for the possible blockage cross-correlation the 360º sweep must be carried out preserving the azimuth spacing, $\Delta\varphi$, between the two satellites.

The use of the street MKFs can also be extended to multiple GSO satellites and to the case of non-GSO constellations. In the last case, the study would consist in the repeated computation of 360º street orientation sweeps for a sufficiently large number of satellite constellation snapshots. A snapshot in this context indicates the instantaneous positions (azimuths and elevations) of the various satellites above a minimum operational elevation, θ_{min}. By defining an appropriate stepping interval, ΔT, and observation period, T_{obs}, the availability can be can be calculated as the time-, street orientation-weighed average of the obtained results in each snapshot. Values of $\Delta T = 1$ min and T_{obs} equal to the constellation period provide adequate results.

FIGURE 15

Calculation of total system availability for a constellation of two GSO satellites with respect to a T-junction